RSC Advances

ROYAL SOCIETY OF CHEMISTRY

www.rsc.org/advances

RSC Advances

ARTICLE

Temperature-controlled morphology evolution of graphitic carbon nitride nanostructures and their photocatalytic activities under visible light

Received 00th January 20xx,
Accepted 00th January 20xx

DOI: 10.1039/x0xx00000x

www.rsc.org/

Quan Gu [a,b,*], Ziwei Gao [a], Hongan Zhao [b], Zaizhu Lou [b], Yusen Liao [b], Can Xue [b,*]

A series of g-C_3N_4 photocatalysts were synthesized by changing the temperature through air-assisted thermal polymerization and etching. The detailed characterization and analysis clearly revealed that the texture, surface structure, optical properties, and band structure of g-C_3N_4 depend on the preparation conditions such as atmosphere and temperature. The morphology of samples obtained at different temperatures undergoes sequential evolution from bulk to nanosheet with multilayer, nanosheet with few layer, moderately rolled nanosheet, tailored nanotube, nanoflakelet and even nanoparticles. Accordingly, the BET surface area increased dramatically from 4.5 m^2/g of bulk g-C_3N_4 to 210.1 m^2/g of modified sample obtained at 540 °C. The different textural and structural properties resulted in the different optical and electronic features. The exfoliated and tailored samples obtained by this method presented better photocatalytic performance as compared with bulk g-C_3N_4. Factors affecting the photocatalytic activity of g-C_3N_4 were discussed in detail on the basis of the textural and structural characterization as well as the photocatalytic activity results. We found that the surface area, surface defects, and light absorption have great impacts on the photocatalytic activities of g-C_3N_4.

1. Introduction

Metal-free semiconductors (such as graphene and its derivatives as well as carbon nitride and $C_3N_3S_3$ organic conjugated polymers) with a great deal of advantages (e.g. non-toxic and abundant) have been developed as photocatalysts.[1-5] Among these semiconductors, graphitic carbon nitride (g-C_3N_4) has been considered as a suitable and promising photocatalyst for the splitting of water into hydrogen or oxygen using solar light. However, condensed bulk g-C_3N_4 cannot give rise to a high photocatalytic performance due to its unsatisfied texture and surface structure. Considering the graphitic structure of g-C_3N_4 and inspired by the discovery and preparation of graphene,[6-8] delaminating, exfoliating, and tailoring the structure of g-C_3N_4 at the nanoscale is a very important research direction in photocatalytic community to change the microstructure and surface property and thus to improve photocatalytic activity of g-C_3N_4, and is also a key to design highly efficient metal free photocatalysts.

As expected, recently, in the research of modification on the microstructure of g-C_3N_4, many breakthrough discoveries have been reported, ranging from bulk to nanosheets, nanotubes, and nanoparticles, from three-dimensional to two-dimensional or zero-dimensional growth. The methods for exfoliating and tailoring laminar structure of g-C_3N_4 include liquid exfoliation,[9-12] hydrothermal approach,[13] protonation,[14] and so on. For example, Zhang et al.[9] utilized ultrasonic exfoliation route in water to prepare the ultrathin g-C_3N_4 nanosheets. The bulk g-C_3N_4 can be also exfoliated in 1, 3-butanediol after ultrasonic processing.[11] Similarly, the crystalline C_3N_4 nanosheets was prepared by one-step liquid exfoliation from layered bulk poly(triazine imide) in water.[10] Wang et al.[14] reported that protonation can breaks up both sheets and stacks, and thus provides a facile method to modify the morphology and microstructure of g-C_3N_4. Besides, heat treatment of bulk g-C_3N_4 in air was also found be an impactful method to achieve the modification of g-C_3N_4.[15,16] All above mentioned methods for exfoliating and tailoring bulk g-C_3N_4 seem a bit complicated, and are consisting of two or more steps including the preparation of bulk g-C_3N_4 and subsequent post-treatment. It should be finding a simple alternative method to attempt one-step preparation to obtain nanosheets and/or tailored g-C_3N_4 by directly precursor heating.

A large number of studies showed that the exfoliation and tailoring of g-C_3N_4 can not only increase the surface area but also influence the surface structure, optical properties, electronic structure and energy band of g-C_3N_4.[9,11,13-15] Moreover, during the exfoliating process by thermal etching both the atmosphere and calcination temperature greatly influence the morphology, structure, and optical properties of as-obtained samples.[15-17] All of these can affect the

[a] Key Laboratory of Applied Surface and Colloid Chemistry, Ministry of Education, School of Chemistry and Chemical Engineering, Shaanxi Normal University, Xi'an, 710062, China;
[b] School of Materials Science and Engineering, Nanyang Technological University, 50 Nanyang Avenue, Singapore 639798; E-mail: cxue@ntu.edu.sg.
† Electronic Supplementary Information (ESI) available: See
DOI: 10.1039/x0xx00000x

photocatalytic activity of g-C_3N_4. Under certain conditions, there are some contradictions between effects of some factors on the photocatalytic activity. For example, after exfoliation, the specific surface area increased but light absorption decreased.[9,11,13,15] Moreover, bandgap narrowing due to the modification of the defects such as nitrogen vacancies leads to the enhanced light absorption but lowered redox ability as a result of the down-shifted conduction band and up-shifted valence band.[18,19] Hence, an in-depth understanding on the main factors influencing the photocatalytic activity of g-C_3N_4 is very important for the synthesis of efficient g-C_3N_4 based photocatalysts.

Herein, in the present work, we use the method of air-assisted thermal polymerization and etching to obtain a series of g-C_3N_4 photocatalyst by changing the calcination temperature, and have systemically investigated the effects of calcination temperature on exfoliation process of g-C_3N_4, morphology evolution, optical properties, band-gap engineering, and photocatalytic activity for water splitting. Factors affecting the photocatalytic activity of g-C_3N_4 are discussed in details on the basis of the textural and structural characterization as well as the photocatalytic activity test. This work not only provides a simple strategy for exfoliating and tailoring bulk g-C_3N_4, but also offers in-depth understanding on structure-activity relationship of graphitic carbon nitride.

2. Experimental

2.1. Preparation of samples

Preparation of bulk g-C_3N_4-W reference

All chemicals used in the experiments were reagent grade and no further purification is needed before use. The bulk g-C_3N_4 reference was synthesized via thermal polycondensation. Typically, 6.0 g melamine was put in a cylindrical alumina crucible (~ 5 cm in diameter) with cover. The crucible was heated up to 520 ^oC for 2 h and then extended to 540 ^oC for 2 h with a heating rate of 5 ^oC min^{-1} in a muffle furnace. The product was finally grounded within a mortar and pestle to get g-C_3N_4 photocatalysts (denoted as g-C_3N_4-W).

Preparation of modified g-C_3N_4

The modified g-C_3N_4 with desired nanoscale and different morphology can be directly synthesized by air-assisted thermal polymerization and etching (denoted as g-C_3N_4-T, where T is the synthesis temperature at 470, 500, 520, and 540 ^oC, respectively). Typically, a certain amount of melamine (6.0 g) was loaded at the centre of an opened combustion boat (alumina crucible with 50 ml volume, 137×27×21 mm). Afterwards the combustion boat was heated to a desired temperature in a muffle furnace for 2 h and then extended to a higher temperature for 2h. After cooling to room temperature, the sample with specific colour and physical condition was deposited on the both ends of crucible boat, where the temperature is lower. The temperature curve versus time and a group of different temperature settings are compiled and shown in Fig. S1 (in supporting information).

2.2. Characterizations

The X-ray diffraction (XRD) patterns of all samples were collected on XRD-6000 X-ray diffractometer (Cu Kα source) at a scan rate of 2^o min^{-1}. Fourier Transform Infrared spectra (FTIR) were derived from Perkin Elmer Fourier Transform Infrared Spectrometer GX. The X-ray photoelectron spectra (XPS) were determined on a VG ESCALAB 250 XPS system with a monochromatized Al Kα X-ray source (15 kV, 200 W, pass energy = 20 eV). The scanning electron microscopy (SEM) images were obtained by JEOL JSM-7600F scanning electron microscope at an acceleration voltage of 5 kV. The transmission electron microscopy (TEM) images were obtained by a JEOL JEM-2010 EX instrument at an accelerating voltage of 200 kV. The N_2 absorption-desorption isotherms were determined at 77 K with a Micromeritics ASAP 2010 instrument. Electron paramagnetic resonance (EPR) signals of samples were examined with a Bruker ESP 300E spectrometer. With Lambda 750 UV/vis/NIR spectrophotometer (Perkin Elmer, USA) using $BaSO_4$ as reference, UV-Vis adsorption was measured. Mott–Schottky curves were measured using a three-electrode system in 0.5 M Na_2SO_4 solution. Photoluminescence (PL) spectra were accomplished in solid with Shimazu RF5301 Spectrofuorophotometer with an excitation wavelength of 380 nm.

2.3. Photocatalytic properties

Photocatalytic H_2 evoluiton

The photocatalytic hydrogen production was carried out in a quartz reactor. Typically, 10 mg of the Pt (3.0 wt.%) loaded sample was dispersed into 10 mL triethanolamine (TEOA, 15 vol.%) aqueous solution. Before the irradiation with visible light, the suspension was degassed with N_2 for 15 minutes to remove the O_2 in the system. A 300 W Xenon Lamp (MAX-302, Asahi Spectra, USA) coupled with a UV cut-off filter (λ > 420 nm) was adopted to provide the visible light. The amount of produced H_2 was analyzed at a regular interval (1 h) by gas chromatograph (Agilent 7890A) with TCD detector. All reactions were accomplished at room temperature.

Photocatalytic O_2 evoluiton

Firstly, The RuO_x cluster loaded samples were prepared by hydrolysis method. Typically, 20 mg as-prepared sample was added to mixture solution containing 25 ml water and 25 ml ethanol with constant stirring for 0.5 h. Then, 20 μL of $RuCl_3$ solution (20 mg Ru/mL) was added under constant stirring for 0.5 h. Subsequently, NaOH solution (0.04 M) was slowly added to adjust the pH to 7 and the mixed solution was then stirred overnight. The products were washed with water and ethanol, dried at 60 ^oC, and finally calcinated at 150 ^oC for 2 h.

Then, the photocatalytic oxygen evolution was carried out in a quartz reactor at room temperature. Typically, 10 mg of the as-prepared RuO_x loaded sample was dispersed into 10 mL $AgNO_3$ (0.1 M) solution. The suspension was degassed with Ar for 15 min to remove the O_2 in the system prior to irradiation under a 300 W xenon lamp (MAX-302, Asahi Spectra, USA) with a UV cut-off filter (λ > 420 nm). The produced O_2 was analyzed at a regular interval (1 h) by gas chromatograph (Agilent 7890A) with TCD detector.

3. Results and discussion

3.1. Evolution of structure and morphology

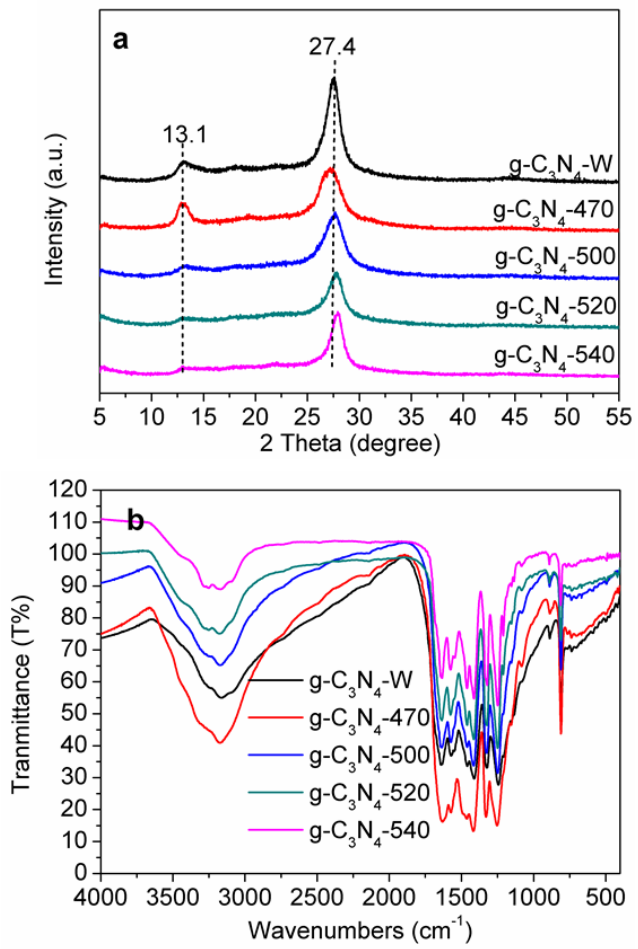

Fig. 1 XRD patterns (a) and FTIR spectra (b) of g-C_3N_4-W reference, g-C_3N_4-470, g-C_3N_4-500, g-C_3N_4-520, and g-C_3N_4-540.

The crystal structure, surface composition and chemical state of as-prepared samples were firstly characterized by XRD, FTIR, and XPS, respectively. Fig. 1a shows XRD patterns of g-C_3N_4-T samples (g-C_3N_4-470, g-C_3N_4-500, g-C_3N_4-520, and g-C_3N_4-540) obtained at different temperature under air atmosphere and bulk g-C_3N_4-W reference prepared by general thermal condensation of melamine. The XRD pattern of the g-C_3N_4-470 presents two diffraction peaks at 13.1° and 27.3°, similar to that of bulk g-C_3N_4-W reference, which are attributed to the in-planar packing and the stacking of the conjugated aromatic system, respectively.[2,20-22] No diffraction peaks belonging to melamine (XRD pattern of melamine is shown in Fig. S2 in supporting information) can be observed. This indicates that the polymerization reaction of melamine can occur at 470 °C to form graphitic carbon nitride, which can be further confirmed by FTIR spectra, as shown in Fig. 1b and S3. The intensity of diffraction peak at 13.1° in XRD pattern of g-C_3N_4-470 is much higher than that of bulk g-C_3N_4-W reference, indicating the perfect g-C_3N_4 structure where the tri-s-triazine unit is connected through bridging nitrogen atoms, as shown in Fig. S4. However, it is found that the XRD peak at 27.3° of g-C_3N_4-470, attributed to packing between the layers, is lower than that of bulk g-C_3N_4-W (27.4°), indicating the larger interlayer distances due to the low degree of condensation and packing between the layers at low heating temperature. With increasing the preparation temperature, the diffraction intensity at the lower angle (13.1°) decreases and the diffraction peak at higher angle (27.4°) shifts to the higher angle. This indicates that the increased heating temperature leads to seriously damage of the periodicity in the parallel direction and a denser packing between the conjugated aromatic systems. Fig. 1b shows the FTIR spectra of g-C_3N_4-470, g-C_3N_4-500, g-C_3N_4-520, g-C_3N_4-540, and g-C_3N_4-W reference. Similar with the g-C_3N_4-W reference, the FTIR spectra of g-C_3N_4-470, g-C_3N_4-500, g-C_3N_4-520, and g-C_3N_4-540 samples display several characteristic bands belonging to the fingerprint region (1200-1650 cm^{-1}) of s-triazine ring (C-NH-C and C=N stretching vibrations), two bands caused by the N-H stretches at 3328 and 3168 cm^{-1}, and a band corresponding to the out of plane bending of the s-triazine ring at 806 cm^{-1}.[17,21] The FTIR spectra of g-C_3N_4-T samples are not changed along with the different preparation temperature. According to the XRD and FTIR results, we can conclude that the g-C_3N_4-T samples also have poly tri-s-triazine structure but with destroyed planar structure and denser interlayer distances.

The XPS analyses results for the g-C_3N_4-T samples and the bulk g-C_3N_4-W reference are shown in Fig. 2. The C 1s signals (Fig. 2a) of all samples can be fitted into two peaks centered at around 284.6, and 288.0 eV, which can be attributed to the aromatic carbon atom and the sp^2 C=N bond in the s-triazine ring, respectively.[15,23-25] As shown in Fig. 2b, the N 1s signals in the binding energy region of 396-402 eV for these samples can be fitted into three peaks located at 398.5 eV, 399.9, and 400.9 eV for sp^2-hybridized nitrogen in triazine rings (C-N=C), tertiary nitrogen N-$(C)_3$ groups, amino functions caring hydrogen (C–N–H), respectively.[26,27] A weak peak of N1s at 404.1 eV for all samples is attributed to charging effects.[26] Comparing to bulk g-C_3N_4-W sample, no obvious binding energy shift of C 1s and N 1s signals for g-C_3N_4-T can be observed, suggesting that the surface chemical states of both C and N in the g-C_3N_4-T samples are the same as in the bulk g-C_3N_4 reference. The binding energies of O 1s peaks at 531.8 and 533.4 eV of bulk g-C_3N_4-W sample (Fig. 2c) are ascribed to adsorbed oxygen species (water and oxygen).[19,28] For g-C_3N_4-T synthesized in an opened crucible, the peak at low binding energy gradually shifted to the higher binding energy along with higher preparation temperature (531.8, 531.9, 532.0, and 532.1 eV for g-C_3N_4-470, g-C_3N_4-500, g-C_3N_4-520, and g-C_3N_4-540, respectively), which might be due to the oxidation some carbon atoms into C=O species at high temperature under air atmosphere.[29] The percentages of elements (C and N) on the surface of various carbon nitride samples are determined by XPS. For g-C_3N_4-470, the surface atomic ratio of C/N is about 0.69, which is close to that of bulk g-C_3N_4-W (0.70). The surface C/N ratio of g-C_3N_4-T increases with increasing of temperature (0.73 for g-C_3N_4-500, 0.81 for g-C_3N_4-520, and 0.82 for g-C_3N_4-540), which suggests that the surface of g-C_3N_4-T obtained at

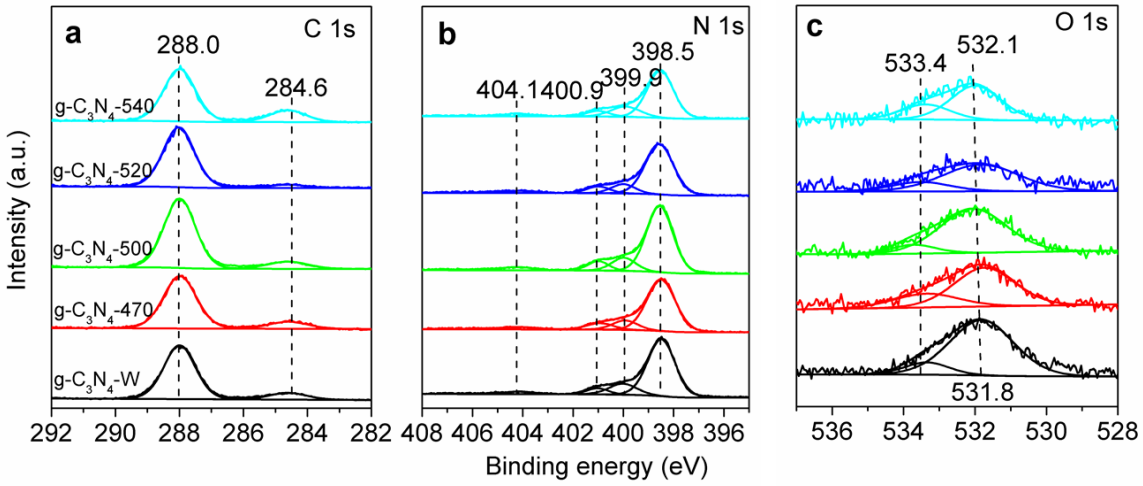

Fig. 2 High resolution XPS spectra of (a) C 1s, (b) N1s, and (c) O1s for bulk g-C_3N_4-W reference, g-C_3N_4-470, g-C_3N_4-500, C_3N_4-520, and g-C_3N_4-540.

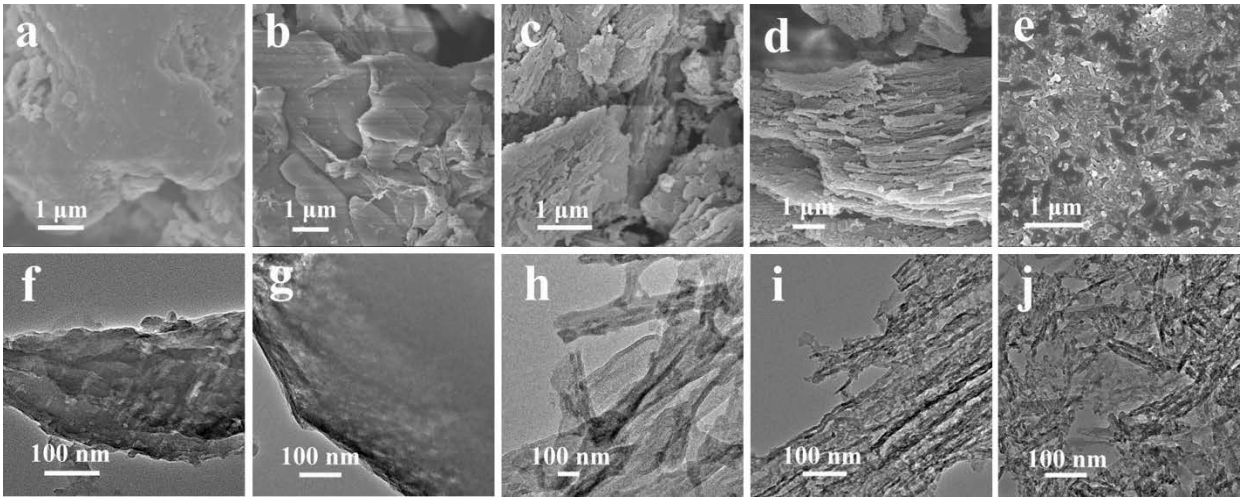

Fig. 3 FESEM and TEM images of bulk g-C_3N_4-W reference (a and f), g-C_3N_4-470 (b and g), g-C_3N_4-500 (c and h), g-C_3N_4-520 (d and i), and g-C_3N_4-540 (e and j), respectively.

high temperature is poor in nitrogen. This is might be due to the thermal oxidation at high temperature, which leads to exfoliation and tailoring of bulk structure of g-C_3N_4. These findings are in good consistence with the XRD, SEM, TEM, and N_2 adsorption results.

The morphology and microstructure of the obtained carbon nitride is changed dramatically with increasing of the preparation temperature. As shown in Fig. 3, the SEM and TEM images of bulk g-C_3N_4 reference (Fig. 3a and f) and g-C_3N_4-470 obtained at lower heating temperature (Fig. 3b and g) represent typical monolith like morphology. When the temperature increased to 500 ^{o}C, the g-C_3N_4-500 became the sheet-like (Fig. 3c and h), suggesting the exfoliation of bulk carbon nitride materials to form the two-dimensional nanosheets by direct heating melamine in air atmosphere. With reaction temperature further increased, nanotube type g-C_3N_4 is synthesized at 520 ^{o}C, which achieves a one-dimensional nanotube growth of g-C_3N_4 (shown in Fig. 3d and i). This indicates that the carbon nitride nanosheets can be rolled up to minimize the surface free energy.[16,30] Additionally, some destroyed tubes and fragments can be observed, indicating the further tailoring by the thermal etching, which can be confirmed by the fact that the tailored nanotubes, nanoflakelets, nanoparticles, even nanodots were formed when the calcination temperature rised up to 540 ^{o}C (Fig. 3e and j).

N_2 adsorption at 77 K was used to further characterize the microstructural change of obtained carbon nitride with increasing the temperature. The N_2 adsorption-desorption isotherm and the corresponding BJH pore-size distribution curve of the g-C_3N_4-T samples and bulk g-C_3N_4-W reference are shown in Fig. 4. The obtained specific BET surface area, pore volume, and pore size of these samples are summarized in Table 1. The specific BET surface area g-C_3N_4-470 sample is relatively low (6.0 cm^2/g), which is highly comparable to that of bulk g-C_3N_4-W reference (4.5 cm^2/g). Accordingly, there

no obvious hysteresis loop observed in the N_2 adsorption-desorption isotherm of g-C_3N_4-470 and bulk g-C_3N_4-W reference (Fig. 4), suggesting that no mesopores in the g-C_3N_4-470 and bulk g-C_3N_4-W reference, which can be confirmed by corresponding BJH pore-size distribution result (inset of Fig. 4). The N_2 adsorption-desorption isotherm of g-C_3N_4-500, g-C_3N_4-520, and g-C_3N_4-540 can be identified as type IV according to the IUPAC classification.[31,32] The obtained specific BET surface area are 41.5, 173.6, and 210.1 cm^2/g, respectively, for g-C_3N_4-500, g-C_3N_4-520, and g-C_3N_4-540 samples, indicating the increased specific BET surface area. For g-C_3N_4-500 sample obtained at 500 °C, the most probable distribution of pore is centered at around 3.5 nm (inset in Fig. 4), which can be attributed to the mesopores between exfoliated carbon nitride nanosheets. When the treatment temperature is further increased, the exfoliated carbon nitride nanosheets rolled up and then the formed nanotubes can be further tailored, therefore the pore distribution centered at 20 nm are observed in the BJH pore-size distribution curves of g-C_3N_4-520 and g-C_3N_4-540 samples, supporting the SEM and TEM observation. These results further confirm that increasing polymerization temperature leads to exfoliation and tailoring of laminar structure of g-C_3N_4. Most importantly, g-C_3N_4 material with mesopores and large surface area can be obtained by using this simple method even though the collection yields decrease at higher preparation temperature (as shown in Table 1). Therefore, according to the results obtained from the SEM, TEM, and N_2 adsorption, we can conclude that the increased temperature in our study gives rise to significant changes in the textural properties of carbon nitride.

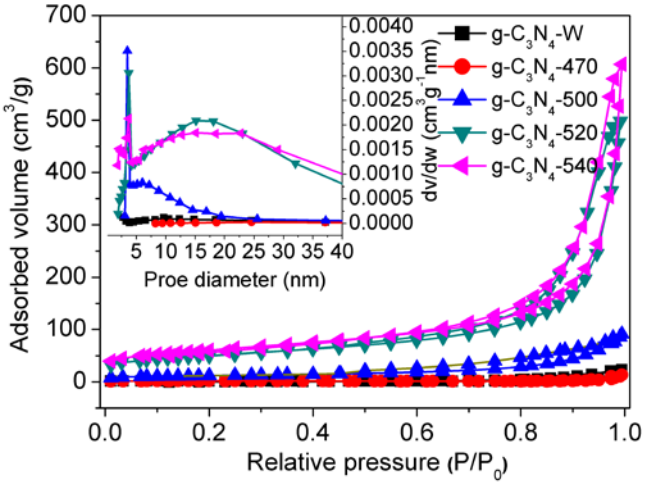

Fig. 4 The N_2 adsorption-desorption isotherm and the corresponding BJH pore-size distribution curve (inset) of bulk g-C_3N_4-W reference, g-C_3N_4-470, g-C_3N_4-500, g-C_3N_4-520, and g-C_3N_4-540, respectively.

3.2. Effects of synthesis temperature on optical property and electronic structure

The optical property and electronic structure of samples were studied by the combined analysis of the electron paramagnetic resonance (EPR), UV-visible absorption spectra, Mott-Schottky, and photoluminescence (PL) spectra. It has been reported that the semiconductor structure of g-C_3N_4 originates from the formation of an extended π-conjugated system composed of s-triazine units.[17] Therefore, the EPR was used to evaluate the semiconductor band structure of g-C_3N_4-T obtained at different preparation temperature. The melamine and melem do not show any observable EPR signal. As shown in Fig. 5a, the EPR spectrum of g-C_3N_4-470 show a signal at g value of 2.003 for the delocalized electrons in the conduction band,[17,33] indicating the polymerization of melamine at 470 °C, which is in agreement with the XRD result (Fig. 1a). The g-C_3N_4-500 sample obtained at 500 °C present stronger signal of at g value of 2.003 as compared to g-C_3N_4-470, suggesting that higher preparation temperature leads to higher polymerization extent.[20,34,35] Further increasing the preparation temperature led to decreased EPR signal intensity because the connected π-conjugated system can be destroyed by thermal exfoliation and tailoring at high temperature under air atmosphere (as shown in Fig. 3), and consequently, the concentration of delocalized electrons in g-C_3N_4 decreases. In comparison, the g-C_3N_4-W reference has very high polymerization extent without exfoliation, thus it exhibit stronger EPR signals than all g-C_3N_4-T samples.

Fig. 5b shows the UV-visible absorption spectra of bulk g-C_3N_4 reference and g-C_3N_4-T samples. The g-C_3N_4-470 sample prepared at lower temperature exhibits an absorption edge at 451 nm, which is shorter than that of bulk g-C_3N_4-W reference (464 nm). This might be due to the low degree of condensation and packing between the layers at low heating temperature.[14,20] Increased preparation temperature leads to the enhanced condensation and packing between the layers, and therefore the obtained g-C_3N_4-500 presents a longer adsorption edge (454 nm), but it is still shorter than that of bulk g-C_3N_4-W reference, which might be due to quantum size effect.[9,17,20,26] With increasing preparation temperature from 500 to 540 °C, the light absorption thresholds of obtained samples gradually shift from 454 to 447 nm (Fig. 5b and Table 1), which should also be attributed to quantum size effect.[9,17,20,26] Fig. 5c shows the Tauc plot as a function of light energy of all samples. According to Fig. 5b and c, the estimated bandgaps are 2.79, 2.87, 2.85, 2.89, and 2.93 eV, corresponding to bulk g-C_3N_4-W reference, g-C_3N_4-470, g-C_3N_4-500, g-C_3N_4-520, and g-C_3N_4-540, respectively, as shown in Table 1. Based on the Mott-Schottky plots (Fig. 5d) The conduction band potentials (E_{CB}) of bulk g-C_3N_4-W reference, g-C_3N_4-470, g-C_3N_4-500, g-C_3N_4-520, and g-C_3N_4-540 are estimated as -1.29 V, -1.26 V, -0.88 V, -1.03 V, and -0.99 V, respectively (Table 1). Accordingly, the band structures of these samples can be depicted as Fig. 5e.

The photoluminescence (PL) spectra of the samples were tested at room temperature with an excitation wavelength of 360 nm. As shown in Fig. 5f, the g-C_3N_4-470 shows a very strong emission peak centered at 448 nm, which is shorter than that of bulk g-C_3N_4-W reference (458 nm), suggesting the lower condensation and packing. This is consistent with the blue-shift of absorption band edge, as shown in Fig. 5b. In addition, the intensity of peak at 448 nm for g-C_3N_4-470 is

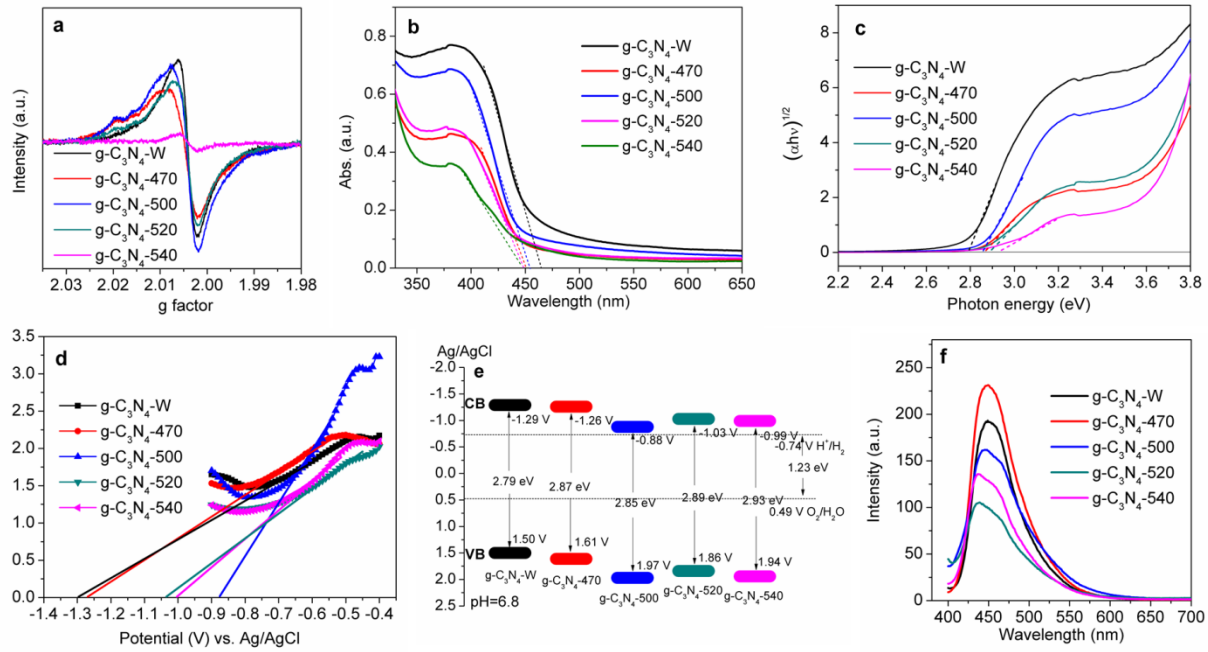

Fig. 5 (a) EPR spectra, (b)UV-vis absorption spectra, (c) Tauc plot, (d) Mott Schoctky, (e) Energy band diagram, and (f) PL spectra of bulk g-C_3N_4-W reference, g-C_3N_4-470, g-C_3N_4-500, g-C_3N_4-520, and g-C_3N_4-540.

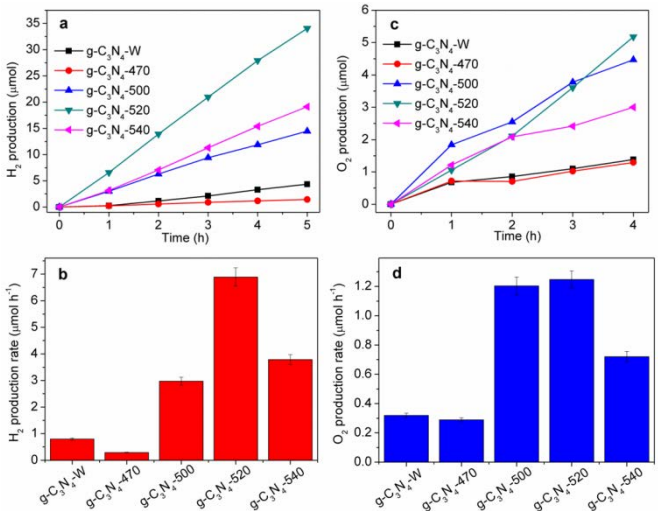

Fig. 6 (a) time resolved hydrogen evolution amount and (b) hydrogen generation rate, (c) time resolved oxygen evolution amount and (b) oxygen generation rate of bulk g-C_3N_4-W reference, g-C_3N_4-470, g-C_3N_4-500, g-C_3N_4-520, and g-C_3N_4-540.

larger than that for g-C_3N_4-W reference, suggesting the strong radiative transition of g-C_3N_4-470. When the preparation temperature increased to 500 °C, the obtained sample showed a red-shifted PL peak at 449 nm, but it is still shorter than that of bulk g-C_3N_4-W reference. The former is due to the enhanced condensation and packing between the layers caused by the increased temperature, and the latter is due to quantum size effect,[9,20] which can be verified by the fact that further increasing preparation temperature leads to the gradual blue-shift of PL peak from 449 to 436 nm (Fig. 5f and Table 1). Increasing preparation temperature from 470 °C to 520 °C leads to the decreased PL intensity, indicating the enhanced non-radiative recombination at trapping states or defects on carbon nitride structure due to the thermal exfoliation and tailoring (shown in SEM and TEM images). However, further increase to 540 °C results in an increase of PL intensity, which might be attributed to the PL of very small g-C_3N_4 nanostructures (Fig. 3e and j) with quantum size effect.[36-38] These results indicate that the fluorescence spectrum of carbon nitride strongly depends on their structure and texture. It is worth noting that the variation of PL intensity of samples is in good agreement with the photocatalytic activity results, suggesting that the structural defects and textural property of samples have great impacts on their photocatalytic performance as discussed in details below.

3.3. Effects of synthesis temperature on photocatalytic activity

The H_2 generation reaction was firstly carried out in an aqueous solution of TEOA (15 vol.%) as the sacrificial agent under visible light (>420 nm) to evaluate the photocatalytic activities of all samples to study the effect of sample preparation temperature on photocatalytic activities. Prior to the photocatalytic test, all samples were loaded with Pt (3.0 wt. %) nanoparticles by using a wetness impregnation method as reported in our previous works.[21,39] The TEM image of Pt-loaded carbon nitride is shown in Fig. S5. Among all modified g-C_3N_4-T samples, g-C_3N_4-470 exhibits the lowest photocatalytic H_2 evolution activity with an H_2 evolution rate of ~0.29 μmol h^{-1}, which is even lower than that of bulk g-C_3N_4 reference (0.80 μmol h^{-1}) due to the bulk structure with low condensation (Fig. 6a and b). A volcano-type histogram of H_2 evolution rate depending on the preparation temperature is observed in Fig. 6b, and the maximum H_2 evolution rate of

Table 1 Summary of the physicochemical characteristics of as-prepared samples.

Samples	Yields	Absorption edge (nm)	Eg (eV)	E_{CB} (V)	E_{VB} (V)	Emission peak (nm)	S_{BET} (cm^2/g)	Pore volume (ml/g)	Pore size (nm)
g-C_3N_4-W	33.4%	464	2.79	-1.29	1.50	458	4.5	0.035	40.2
g-C_3N_4-470	40.7%	451	2.87	-1.26	1.61	448	6.0	0.02	35.2
g-C_3N_4-500	16.2%	454	2.85	-0.88	1.97	449	41.5	0.14	9.2
g-C_3N_4-520	1.70%	448	2.89	-1.03	1.86	439	173.6	0.77	15.6
g-C_3N_4-540	0.35%	447	2.93	-0.99	1.94	436	210.1	0.94	16.5

6.89 μmol h^{-1} is achieved on the g-C_3N_4-520 sample prepared at 520 °C, which is nearly 24 times higher than that of g-C_3N_4-470. It is worth noting that the photocatalytic H_2 evolution rates of the all exfoliated and tailored samples (2.97 μmol h^{-1}, 6.89 μmol h^{-1}, and 3.79 μmol h^{-1} for g-C_3N_4-500, g-C_3N_4-520, and g-C_3N_4-540, respectively) are higher than that of bulk g-C_3N_4 reference, suggesting that the thermal exfoliation and tailoring for carbon nitride are effective for improving the photocatalytic H_2 evolution activity.

Then, we also evaluated the photocatalytic O_2 evolution of RuO_x clusters (2.0 wt. %) loaded carbon nitride samples (Fig. S6, see supporting information) from aqueous solution with $AgNO_3$ as the sacrificial agent under visible light irradiation. The results are shown in Fig. 6c and d. All samples exhibit visible light activity for O_2 evolution, although the order of magnitude for O_2 evolution rates is lower than that for H_2 evolution (comparison between Fig. 6b and d). Similar to H_2 evolution, the O_2 evolution rates increase with increasing preparation temperature from 470 °C to 520 °C and reach a maximum at 520 °C, followed by a decrease when the temperature increases to 540 °C. The g-C_3N_4-470 sample with bulk structure also shows the lowest O_2 evolution rate (0.28 μmol h^{-1}). The exfoliated and tailored samples present the enhanced photocatalytic O_2 evolution activity (1.20 μmol h^{-1}, 1.24 μmol h^{-1}, and 0.72 μmol h^{-1} for g-C_3N_4-500, g-C_3N_4-520, and g-C_3N_4-540, respectively) as compared to g-C_3N_4-W reference (0.32 μmol h^{-1}).

3.4. Factors affecting the photocatalytic activity

XRD, FTIR, XPS, SEM, TEM, and N_2 adsorption results showed that the polymerization conditions such as the atmosphere, vapour pressure, and polymerization temperature have great influences on textural and structural properties of graphitic carbon nitride. When the melamine precursor was sealed in a cylindrical alumina crucible, because of the lower concentration of oxygen, flowability of produced gases (such as NH_3, CO, and CO_2 etc.) during the polymerization process and vapor pressure of melamine, the g-C_3N_4 reference obtained at 520 °C with stone-like morphology has very low specific surface area, as shown in Fig. 3, 4 and Table 1. If the precursor is placed on an opened combustion boat, the polymerization of melamine takes place in air atmosphere and thus the sample obtained at same temperature (520 °C) exhibits very different microstructure with tube like morphology, which might be due to the evaporation of precursor, flowing of produced gases, and thermal etching of oxygen, and thus has very large surface area (173.6 m^2/g) compared to the bulk g-C_3N_4 reference (4.5 m^2/g). The photocatalytic activity (both H_2 evolution and O_2 evolution) of g-C_3N_4-520 sample is much better than that of the bulk g-C_3N_4-W reference obtained at same temperature. We also found that the temperature has great impact on the polymerization and thermal etching process. The morphology of samples obtained at different temperatures undergoes sequential evolution from bulk to nanosheet with multilayer, nanosheet with few layer, moderately rolled nanosheet, tailored nanotube, and even nanodots. Accordingly, the specific surface area of samples increases gradually with increasing of temperature. The S_{BET} of g-C_3N_4-470, g-C_3N_4-500, g-C_3N_4-520, and g-C_3N_4-540 samples are 6.0, 41.5, 173.6 and 210.1 cm^2/g, respectively, as shown in Table 1. For g-C_3N_4-470, g-C_3N_4-500, and g-C_3N_4-520 samples, their photocatalytic activities increase with larger specific surface area (Fig. 6). Based upon the above analyses, we can conclude that the surface area is a very important factor influencing the photocatalytic activity of graphitic carbon nitride. The exfoliated and tailored structure can shorten the migration distance of photogenerated charge carriers, which is beneficial to reduce the chance of charge recombination. In addition, the larger surface area can also provide more surface active sites for reactions.

During the process of heat treatment, the layer structure can be gradually exfoliated and the conjugated poly-triazine ring structure is damaged to a certain extent (as shown in Fig.3). Accordingly, the g-C_3N_4 surface structure will be changed, such as increased surface defects, which can be confirmed by PL results (Fig. 5f). The photocatalytic activity results showed that surface defects are helpful to improve the activity because the surface defects can capture the photogenerated carriers, inhibiting the radiative recombination (as shown in PL spectra). But redundant defects can act as recombination centers of photogenerated charge carriers, promoting charge recombination and thus reducing the photocatalytic activity. This can be proved by the fact that the g-C_3N_4-540 sample exhibits reduced photocatalytic activities.

The different textural and structural properties result in the different optical and electronic characterization (EPR, UV-Vis absorption, Mott Schoctky, and PL), as shown in Fig. 5. Light absorption of semiconductor photocatalyst is also one of the important factors affecting the photocatalytic activity. Generally, the longer optical absorption edge allows more light be absorbed by the materials and thus leads to the enhanced photocatalytic activity. Because of the low polymerization degree, g-C_3N_4-470 sample shows the narrow light absorption range as compared to the bulk g-C_3N_4-W reference, which is also one of the reasons for its low activity. As shown in SEM and TEM images (Fig. 3), the size and thickness of g-C_3N_4 gradually decrease as a result of the thermal cutting and stripping effect. Therefore, the optical absorption edge of g-C_3N_4-500, g-C_3N_4-520, and g-C_3N_4-540 samples shift to short wavelength as compared to g-C_3N_4-W reference and further gradually blue shift to with increasing of temperature (Fig. 5b and c) due to the quantum effect. The activity results indicate that their activities displayed a volcano-type of H_2 and O_2 evolution rates instead of linear decrease. But the photocatalytic activities of each sample (g-C_3N_4-500, g-C_3N_4-520, and g-C_3N_4-540) are still much higher than that of bulk C_3N_4-W reference. Hence one can see that only when the temperature is increased up to 540, effects of light absorption on the photocatalytic activity predominated. So, the reasons for decreased photocatalytic activity of g-C_3N_4-540 sample with the largest specific surface area are attributable to the too many surface defects as the recombination centers and the blue shift of absorption edge.

Conclusions

In summary, the modified g-C_3N_4 photocatalysts with exfoliated and tailored structure are successfully obtained by using air-assisted thermal polymerization and etching. The effects of calcination temperature on exfoliation process of g-C_3N_4, morphology evolutions, optical properties, band-gap engineering, and photocatalytic activity for water splitting are systemically studied and clarified. The morphology of samples obtained at different temperatures undergoes sequential evolution from bulk to nanosheet with multilayer, nanosheet with few layer, moderately rolled nanosheet, tailored nanotube, and nanoflakelet even nanoparticles. The samples prepared at different temperatures also have different surface structure, optical properties, and energy band structures. The exfoliated and tailored samples obtained by this method present better photocatalytic activities as compared to that of bulk g-C_3N_4. On the basis of the textural and structural characterization as well as the photocatalytic activity results, we can conclude that the surface area, surface defects, light absorption have great effects on the photocatalytic activity of g-C_3N_4.

Acknowledgements

This work was financially supported by NTU seed funding for Solar Fuels Laboratory, MOE AcRF-Tier1 (RG 44/11), MOE AcRF-Tier2 (MOE2012-T2-2-041, ARC 5/13), and CRP (NRF-CRP5-2009-04) from NRF Singapore.

Notes and references

1 Q. Xiang, J. Yu and M. Jaroniec, *Chem. Soc. Rev.,* 2012, **41**, 782.
2 X. Wang, K. Maeda,A. Thomas, K. Takanabe, G. Xin, J. M. Carlsson, K. Domen and M. Antonietti, *Nat. Mater.,* 2009, **8**, 76.
3 Y. P. Yuan, L. S. Yin, S. W. Cao, L. N. Gu, G. S. Xu, P. W. Du, H. Chai, Y. S. Liao and C. Xue, *Green Chem.* 2014, **16**, 4663.
4 J. Xu, L. Luo, G. Xiao, Z. Zhang, H. Lin, X. Wang and J. Long, *ACS Catal.,* 2014, **4**, 3302.
5 J. Liu, Y. Liu, N. Liu, Y. Han, X. Zhang, H. Huang, Y. Lifshitz, S.-T. Lee, J. Zhong and Z. Kang, *Science,* 2015, **347**, 970.
6 D. A. Dikin, S. Stankovich, E. J. Zimney, R. D. Piner, G. H. B. Dommett, G. Evmenenko, S. T. Nguyen and R. S. Ruoff, *Nature,* 2007, **448**, 457.
7 J. Shen, Y. Hu, M. Shi, X. Lu, C. Qin, C. Li and M. Ye, *Chem. Mater.,* 2009, **21**, 3514.
8 W. Zhao, M. Fang, F. Wu, H. Wu, L. Wang and G.Chen, *J. Mater. Chem.,* 2010, **20**, 5817.
9 X. Zhang, X. Xie, H. Wang, J. Zhang, B. Pan and Y. Xie, *J. Am. Chem. Soc.,* 2013, **135**, 18.
10 K. Schwinghammer, M. B. Mesch, V. Duppel, C. Ziegler, J. Senker and B. V. Lotsch, *J. Am. Chem. Soc.* 2014, **136**, 1730.
11 X. She, H. Xu, Y. Xu, J. Yan, J. Xia, L. Xu, Y. Song, Y. Jiang, Q. Zhang and H. Li, *J. Mater. Chem. A,* 2014, **2**, 2563.
12 S. Yang, Y. Gong, J. Zhang, L. Zhan, L. Ma, Z. Fang, R. Vajtai, X. Wang and P. M. Ajayan, *Adv. Mater.,* 2013, **25**, 2452.
13 T. Sano, S. Tsutsui, K. Koike, T. Hirakawa, Y. Teramoto, N. Negishi and K. Takeuchi, *J. Mater. Chem. A,* 2013, **1**, 6489.
14 Y. Zhang, A. Thomas, M. Antonietti and X. Wang, *J. Am. Chem Soc.,* 2009, **131**, 50
15 P. Niu, L. Zhang, G. Liu and H.-M. Cheng, *Adv, Funct. Mater.,* 2012, **22**, 4763.
16 S. Wang, C. Li, T. Wang, P. Zhang, A. Li and J. Gong, *J. Mater. Chem. A,* 2014, **2**, 2885.
17 J. Sun, J. Zhang, M. Zhang, M. Antonietti, X. Fu and X. Wang, *Nat. Commun.,* 2012, 1139.
18 P. Niu, L.-C. Yin, Y.-Q. Yang, G. Liu and H.-M. Cheng, *Adv. Mater.,* 2014, **26**, 8046.
19 J. Li, B. Shen, Z. Hong, B. Lin, B. Gao and Y. Chen, *Chem. Commun.,* 2012, **48**, 12017.
20 Y. Wang, X. Wang and M. Antonietti, *Angew. Chem. Int. Ed.,* 2012, **51**, 68.
21 Q. Gu, Y. Liao, L. Yin, J. Long, X. Wang and C. Xue, *Appl. Catal. B: Environ.,* 2015, **165**, 503.

22 K. Maeda, R. Kuriki, M. Zhang, X. Wang and O. Ishitani, *J. Mater. Chem. A,* 2014, **2**, 15146.
23 Y. P. Yuan, W. T. Xu, L. S. Yin, S. W. Cao, Y. S. Liao, Y. Q. Tng and C. Xue, *Int. J. Hydrogen Energy*, 2013, **38**, 13159.
24 J. Ding, Q. Liu, Z. Zhang, X. Liu, J. Zhao, S. Cheng, B. Zong and W.-L. Dai, *Appl. Catal. B: Environ.,* 2015, **165**, 511.
25 L. S. Yin, Y. P. Yuan, S. W. Cao, Z. Y. Zhang and C. Xue, *RSC Adv.*, 2014, **4**, 6127.
26 J. Zhang, M. Zhang, C.Yang and X. Wang, *Adv. Mater.,* 2014, **26**, 4121.
27 S. W. Cao, X. F. Liu, Y. P. Yuan, Z. Y. Zhang, J. Fang, S. C. J. Loo, J. Barber, T. C. Sum and C. Xue, *Phys. Chem. Chem. Phys.*, 2013, **15**, 18363.
28 D. Wei, Y. Liu, Y. Wang, H. Zhang, L. Huang and G. Yu, *Nano Lett.,* 2009, **9**, 1752.
29 F. Xiao, J. Miao, and B. Liu, *J. Am. Chem. Soc.,* 2014, **136**, 1559.
30 P. Cendula, S. Kiravittaya, I. Mönch, J. Schumann and O. G. Schmidt, *Nano Lett.,* 2011, **11**, 236.
31 C. Yuan, X. Zhang, L. Su, B. Gao and L. Shen, *J. Mater. Chem.,* 2009, **19**, 5772.
32 A. Vinu, *Adv. Funct. Mater.,* 2008, **18**, 816.
33 Y. Zhang, Z. Schnepp, J. Cao, S. Ouyang, Y. Li, J. Ye and S. Liu, *Sci. Rep.,* 2013, **3***,* 2163; DOI:10.1038/srep02163.
34 V. W.-h. Lau, M. B. Mesch, V. Duppel, V. Blum, J. Senker and B. V. Lotsch, *J. Am. Chem. Soc.,* 2015, **137**, 1064.
35 M. J. Bojdys, J.-O. Müller, M. Antonietti and A. Thomas, *Chem.-Eur. J.,* 2008, **14**, 8177.
36 J. Zhou, Y. Yang, and C-Y. Zhang, *Chem. Comm.,* 2013, **49**, 8605.
37 S. Barman and M. Sadhukhan, *J. Mater. Chem.,* 2012, **22**, 21832.
38 S. Liu, J. Tian, L. Wang, Y. Luo, and X. Sun, *RSC Adv.,* 2012, **2**, 411.
39 Q. Gu, J. Long, H. Zhuang, C. Zhang, Y. Zhou and X. Wang, *Phys. Chem. Chem. Phys.,* 2014, **16**, 12521.